Radiochemistry, Vol. 47, No. 3, 2005, pp. 215–224. Translated from Radiokhimiya, Vol. 47, No. 3, 2005, pp. 193–202.
Original Russian Text Copyright © 2005 by Yu. Teterin, Maslakov, Ryzhkov, Traparić, Vukčević, A. Teterin, Panov.

Nature of the Chemical Bond in Uranium Dioxide UO_2

Yu. A. Teterin*, K. I. Maslakov*, M. V. Ryzhkov, O. A. Traparić***, L. Vukčević****, A. Yu. Teterin*, and A. D. Panov***

** Russian Research Centre Kurchatov Institute, Moscow, Russia*
*** Institute of Solid State Chemistry, Russian Academy of Sciences, Ural Division, Yekaterinburg, Russia*
**** Spika Institute, Trebinje, Republic of Serbia, Bosnia and Herzegovina*
***** University of Montenegro, Podgorica, Serbia and Montenegro*

Received May 17, 2004

Abstract—Fine structure of the X-ray photoelectron and conversion spectra of low-energy (0–40 eV) electrons of uranium dioxide UO_2 was analyzed based on the electronic structure calculations for the UO_8^{12-} cluster with O_h symmetry, simulating the nearest surrounding of uranium in UO_2, by the relativistic X_α discrete variation method. It was predicted theoretically and validated experimentally that, in UO_2, the U5*f* electrons (~1 U5*f* electron) can directly participate in chemical bonding: ~2 U5*f* electrons weakly contributing to chemical bonding are localized at –1.9 eV; ~1 U5*f* electron participating in chemical bonding is delocalized in the range of outer valence molecular orbital energies from –4 to –9 eV; and unfilled U5*f* states are localized mostly at low (from 0 to 5 eV above zero) energies. It was shown experimentally that the U6*p* electrons actively participate in formation of not only inner valence but also outer valence (0.6 U6*p* electron) molecular orbitals. The density of the U6*p* states in UO_2 was estimated experimentally. The composition and sequence of the inner valence molecular orbitals at energies within 13–40 eV were also elucidated.

X-ray photoelectron spectroscopic (XPS) studies of uranium oxides showed that the spectra of low-energy electrons in UO_2 and UO_3 at binding energies E_b within 0–40 eV markedly differ in the structure [1–4]. The U(VI) ion in the trioxide UO_3 has the electronic configuration $\{Rn\}5f^0$, and the U(IV) ion in the dioxide UO_2, the $\{Rn\}5f^2$ configuration (where {Rn} is the electronic configuration of radon), and the X-ray photoelectron spectrum of UO_2, by contrast to UO_3, exhibits at $|E_b|$ = 1.9 eV a fairly narrow intense line of U5*f* electrons weakly contributing to the chemical bonding.

Also, at low binding energies (within 0–40 eV) of electrons of uranium oxides and other actinide compounds, the lines observed have, for the most part, a width of several electron-volts. This is in many cases larger than the width of the lines of electrons from deeper-lying inner shells [5]. For example, the half-width Γ, eV, of the line of the O1*s* electrons ($|E_b|$ = 530.5 eV) of UO_2 was estimated at 1.6 eV, while that of the O2*s* electrons ($|E_b|$ = 23.3 eV), at 4 eV, and this line has a fine structure [3, 4]. These data contradict the indeterminacy relationship $\Delta E\Delta\tau \sim h/2\pi$, where ΔE is the natural width of the level from which a photoelectron was removed; $\Delta\tau$, lifetime of the hole state of the ion formed; and *h*, Planck's constant. Indeed, the lifetime of the hole $\Delta\tau$ tends to decrease with increasing absolute value of the level energy, and the lines in the X-ray photoelectron spectra of separate atoms should become narrower with decreasing binding energy of the electrons. In the case of UO_2 and UO_3, the situation is the opposite. This stimulated extensive theoretical and experimental studies on the nature of the chemical bonding in actinide compounds. These studies showed that one reason for broadening of the lines in the X-ray photoelectron spectra in the region of low binding energies of electrons of actinides in compounds is formation of outer valence molecular orbitals (OVMOs) with energies from 0 to ~13 eV and inner valence MOs (IVMOs) with energies from ~13 to ~50 eV with active participation of the filled An6*p* atomic shells of actinides [4]. These spectra essentially reflect the structure of the valence band (from 0 to 50 eV) and are represented by bands with widths of several electron-volts. More recent studies [5] showed that, under appropriate conditions, inner valence MOs can be formed in compounds of all elements.

Previously, it was commonly believed that the An5*f* electrons involved in chemical bonding are preliminarily excited to, e.g., the An6*d* atomic orbitals. At the same time, calculations showed that the An5*f* shells of the atoms can directly participate in formation of the MOs of actinide compounds [6–8]. This is of principal importance and needs experimental verification. The validity of the electronic structure calculations for actinide compounds can be judged from comparison of the theoretical and experimental partial densities of the An5*f* and An6*p* electrons.

1066-3622/05/4703-0215© 2005 Pleiades Publishing, Inc.

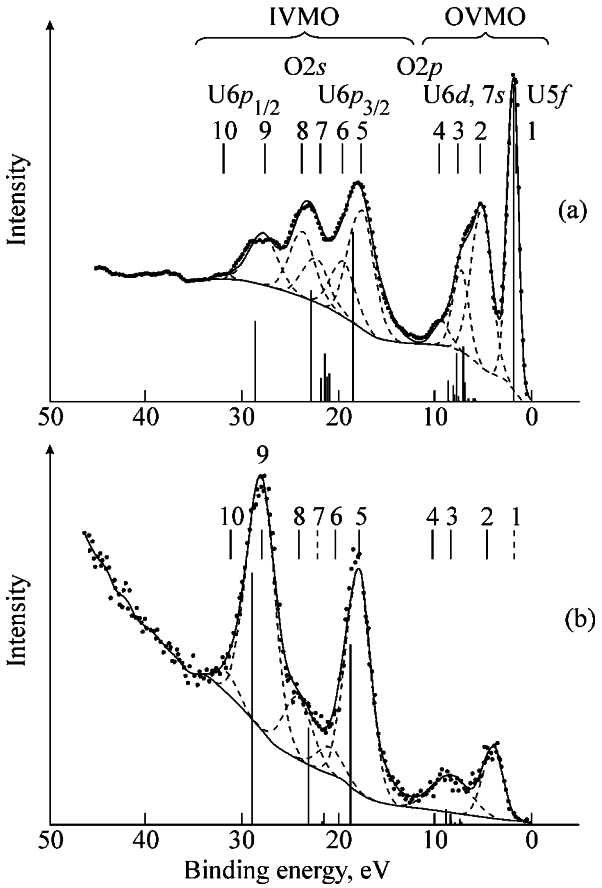

Fig. 1. (a) X-ray photoelectron and (b) conversion electron spectrum of UO_2. Vertical lines under the spectra represent the corresponding theoretical spectra. The contour of the subtracted background is shown, and resolution of the spectra into individual components is illustrated. The intensity in the experimental spectra is given in arbitrary units, and that of the theoretical spectra is normalized in %.

The qualitative analysis of the structure of the X-ray photoelectron spectra of uranium oxides [3, 4] allowed tentative identification of the lines in the conversion electron [9–11] and high-resolution $O_{4,5}$(U) X-ray emission [12] spectra of UO_2 and UO_3. These findings provide additional experimental evidence of formation of IVMOs in uranium oxides. Correct analysis of the fine structure of the X-ray photoelectron, conversion, and $O_{4,5}$(U)-emission spectra of UO_2 and UO_3 was precluded by the lack of the results of relativistic calculations of their electronic structure. For UO_3, such calculations were recently carried out, which allowed full identification of the fine structure of the X-ray photoelectron and conversion spectra of this oxide [13, 14].

In this study, we analyzed the fine structure of the low-energy X-ray photoelectron and conversion electron spectra of UO_2 at electron binding energies within 0–40 eV. To this end, we utilized the results of relativistic calculations by the X_α discrete variation method (RX_α-DVM) of the electronic structure of the UO_8^{12-} cluster with O_h symmetry, simulating the nearest surrounding of uranium in UO_2.

EXPERIMENTAL AND CALCULATION TECHNIQUES

The X-ray photoelectron spectrum of UO_2 was recorded at room temperature on an HP5950A electrostatic spectrometer using $AlK_{\alpha_{1,2}}$ ($h\nu$ = 1486.6 eV) monochromated exciting radiation in a 1.3×10^{-7} Pa vacuum and a low-energy electron gun to compensate the electrostatic charging of the sample during photoemission of photoelectrons from its surface. The resolution of the spectrometer was estimated at 0.8 eV from the halfwidth of the line of the $Au4f_{7/2}$ electrons. The binding energies E_b, eV, are referenced to that of the C1*s* electrons of hydrocarbons on the sample surface, taken equal to 285.0 eV. On a gold substrate, E_b(C1*s*) = 284.7 eV and $E_b(Au4f_{7/2})$ = 83.8 eV [4]. The spectrum of the O1*s* electrons of UO_2 was represented by a single line with a halfwidth Γ = 1.6 eV. At the same time, the halfwidth of the line of the C1*s* electrons of the hydrocarbons was 1.3 eV. The binding energies of the electrons and line widths were determined accurately to within 0.1 eV, and relative line intensities, to 10%.

The $UO_{2.06}$ sample for the X-ray photoelectron study was a dense thick layer with a mirror surface. It was prepared from a finely dispersed powder by grinding in an agate mortar and pressing into indium on a metal support. The characteristics of the X-ray photoelectron spectrum of this sample (electron binding energies) were identical, within the measurement error, to those of UO_2 formed on the metal plate surface [4]. In measurements of the conversion electron spectrum on the same spectrometer, utilizing an additional electron accelerating system, we used an indium substrate for implantation of the uranium isomer by electrostatic collection in an oxygen atmosphere of the ^{235m}U recoil atoms yielded by α-decay of ^{239}Pu [11]. The lines were identified and the conversion spectrum was calibrated on the basis of the X-ray photoelectron spectrum of UO_2. The spectral background due to elastically scattered electrons was subtracted from the X-ray photoelectron spectrum by the Shirley technique [15]. In the case of the conversion electron spectrum, this background was subtracted both by the Shirley technique and by exponent [11]. The relative intensities of the lines differed by no more than 5%. Figure 1 demonstrates the conversion electron spec-

trum, from which the background was subtracted by exponent.

The UO_8^{12-} cluster with O_h symmetry, simulating the nearest surrounding of uranium in UO_2, is a body-centered cube with an edge of 2.74 Å and a bond length R_{U-O} = 2.373 Å, whose center is occupied by the uranium atom, and apices, by eight oxygen atoms (ligands L) [16]. The calculations for this cluster were carried out in the relativistic approximation by the X_α discrete variation method [17, 18], based on solving the Dirac–Slater equation for four-component spinors with the correlation exchange potential [19]. The extended basis of numerical atomic orbitals obtained by solving the Dirac–Slater equation for isolated atoms included, along with filled, vacant states U7$p_{1/2}$ and U7$p_{3/2}$. Also, the basis took into account the cluster symmetry: Using the projection operator technique [17], we obtained linear combinations of ordinary atomic orbitals AOs, transformed by irreducible representations of the O_h double group. The relativistic basis sets were obtained using an original symmetrization routine utilizing the irreducible representation matrices of the majority of the double groups from [19] and the transformation matrices from [20, 21]. Numerical Diophantine integration in calculating the matrix elements of the secular equation was carried out using a set of 22000 points spread over the cluster space, which afforded agreement of the energies of the molecular orbitals no worse than within 0.1 eV. The local correlation exchange potential was in the X_α form with the parameter α equal to the weighted average of the atomic parameters. Since the clusters were fragments of a crystal, the self-consistency was achieved by utilizing the procedure of renormalization of the population densities of the valence AOs of the ligands. This procedure takes due account of the stoichiometry of the compound and the pattern of charge redistribution between the ligands and the surrounding crystal. To correctly estimate the combined influence of all the relativistic effects in UO_2, we carried out nonrelativistic calculation by the X_α discrete variation method for this cluster with identical crystallographic and calculation parameters.

RESULTS AND DISCUSSION

The X-ray photoelectron spectrum of low-energy electrons (0–40 eV) of UO_2 can be arbitrarily divided in two parts (Fig. 1). The first part at energies within 0–13 eV exhibits a structure due to electrons of the OVMOs formed mostly by the outer valence U5*f*, 6*d*, 7*s* and O2*p* AOs of the neighboring atoms, incompletely filled with electrons (Table 1). The second part of the spectrum at energies within 13–40 eV exhibits a fine structure due to electrons of the IVMOs. These orbitals mostly arise from strong interaction of electrons of the completely filled inner valence U6*p* and O2*s* AOs of the nearest U and O atoms. The strong correlation of the spectral parameters of the IVMO part of the spectrum with the structure of the nearest surrounding of uranium in various compounds was the reason for division of the MOs of interest into OVMOs and IVMOs [4, 5]. The X-ray photoelectron spectrum of the OVMO electrons exhibits characteristic features and can be resolved into four components. In the region of the IVMO electrons, the spectrum contains prominent maxima and can be resolved into six components (Fig 1). Formal as it is, this resolution of the spectra into components allows qualitative and quantitative comparison of the characteristics of the X-ray photoelectron spectrum with those of the conversion electron spectrum and with the results of the relativistic calculation of the electronic structure of the UO_8^{12-} cluster with the O_h symmetry.

Table 1 presents the results of the relativistic calculations of the electronic structure for the ground state of the UO_8^{12-} cluster and the composition of the MOs. After photoemission of the electron, the molecule changes into an excited state with a hole in an individual level, and more rigorous comparison of the experimental and theoretical binding energies of the electrons utilizes the calculated values for the transition state [24]. However, it can be roughly assumed that, in the valence band, the electron binding energies calculated for the transition state are constantly shifted to energies of larger absolute value compared to those of the ground state. Therefore, to compare the calculated and experimental binding energies, we increased in this work the corresponding theoretical values by 1.9 eV (Table 2). Taking into account the composition of the MOs (Table 1) and photoionization cross sections ([22], the σ_i parameters for the U7*p* electrons were calculated by V.G. Yarzhemskii), we determined the theoretical intensities for the individual ranges of the spectrum (Table 2, Fig. 1). Comparison of the experimental X-ray photoelectron spectrum with the theoretical data should take into account the fact that the X-ray photoelectron spectrum of UO_2 reflects the band structure and consists of bands broadened due to solid-state effects. Despite approximations used in the calculations, the theoretical and experimental data agree satisfactorily. Indeed, the theoretically predicted widths and relative intensities of the outer valence and inner valence bands are comparable with those derived

Table 1. Composition (fractions) and energies E_0,* eV, of the MOs of the UO_8^{12-} cluster for R_{U-O} = 2.37 Å (RX_α–DVM), photoeffect cross sections σ_i**, and one-electron partial conversion probabilities α_i***

MO	Q	$-E_0$, eV	Composition of MO												
			U										O		
			6*s* 1.14 0.07	$6p_{1/2}$ 0.89 49.38	$6p_{3/2}$ 1.29 23.55	$6d_{3/2}$ 0.61 6.55	$6p_{5/2}$ 0.55 7.71	7s 0.12 0.01	$5f_{5/2}$ 3.67 0.07	$5f_{7/2}$ 3.48 0.04	$7p_{1/2}$ 0.07 8.23	$7p_{3/2}$ 0.10 4.39	2*s* 0.96	$2p_{1/2}$ 0.07	$2p_{3/2}$ 0.07
OVMO															
$8\gamma_7^+$	0	–6.09					0.84						0.04	0.10	0.02
$14\gamma_8^+$	0	–5.85				0.42	0.41						0.04	0.02	0.11
$11\gamma_6^+$	0	–4.18						0.90					0.05	0.02	0.03
$13\gamma_8^+$	0	–2.33				0.39	0.47							0.04	0.10
$16\gamma_8^-$	0	–1.78							0.01	0.01		0.91	0.03		0.04
$12\gamma_6^-$	0	–1.52									0.92		0.03	0.04	0.01
$8\gamma_7^-$	0	–1.50							0.12	0.75			0.01	0.06	0.06
$11\gamma_6^-$	0	–0.77								0.94				0.06	
$15\gamma_8^-$	0	–0.73								0.81		0.15	0.01	0.01	0.02
$7\gamma_7^-$	0	–0.08							0.78	0.16				0.01	0.05
$14\gamma_8^-$	2	0.00							0.92			0.01			0.07
$13\gamma_8^-$	4	3.97												0.32	0.68
$12\gamma_8^+$	4	4.14												0.16	0.84
$10\gamma_6^+$	2	4.19												0.66	0.34
$7\gamma_7^+$	2	4.60												0.13	0.87
$11\gamma_8^+$	4	4.62												0.43	0.57
$10\gamma_6^-$	2	4.93		0.01						0.05	0.05			0.89	
$11\gamma_8^-$	4	5.08			0.02					0.01		0.02		0.21	0.74
$12\gamma_8^-$	4	5.16			0.02				0.06	0.01		0.05		0.03	0.83
$6\gamma_7^-$	2	5.19							0.06	0.06				0.30	0.58
$9\gamma_6^-$	2	5.69		0.01						0.01	0.01				0.97
$10\gamma_8^-$	4	5.81							0.03	0.04				0.18	0.75
$5\gamma_7^-$	2	5.83							0.04	0.02				0.63	0.31
$6\gamma_7^+$	2	6.10					0.11						0.02	0.76	0.11
$9\gamma_6^+$	2	6.16	0.01					0.04					0.02	0.32	0.61
$10\gamma_8^+$	4	6.19				0.07	0.05						0.02	0.08	0.78
$9\gamma_8^+$	4	6.72				0.08	0.10							0.25	0.57
IVMO															
$9\gamma_8^-$	4	16.60			0.63							0.01	0.33	0.01	0.02
$4\gamma_7^-$	2	19.11							0.01	0.01			0.98		
$8\gamma_6^-$	2	19.30		0.04							0.03		0.93		
$5\gamma_7^+$	2	19.51					0.06						0.94		
$8\gamma_8^+$	4	19.51				0.03	0.02						0.95		
$8\gamma_6^+$	2	19.94	0.01					0.06					0.93		
$8\gamma_8^-$	4	20.93			0.34							0.01	0.63	0.01	0.01
$7\gamma_6^-$	2	26.73		0.95									0.04		0.01
$7\gamma_6^+$	2	43.27	0.99										0.01		

Notes: The upper filled molecular orbital is $14\gamma_8^-$ (2 electrons); the filling number for $n\gamma_6^+$ and $n\gamma_7^+$ MOs is 2, and that for $n\gamma_8{}^+$ MO, 4 electrons. The same for Table 2.

* The calculated energies are shifted downward to negative values by 7.5 eV in the absolute value.

** The photoionization cross sections σ_i, kb, per electron were taken from [22] and are given under the AO designations (the first figure).

*** Relative partial probabilities of conversion α, %, of the *E*3 multipole of the ^{235}U nucleus with participation of electrons from n_{lj} shells for the U(IV) ion were obtained using the data from [23] and are given under the AO designations (the second figure).

Table 2. Characteristics of the X-ray photoelectron and conversion spectra of the UO_8^{12-} cluster (O_h) for R_{U-O} = 2.37 Å (RX_α-DVM) and state density of the U6*p* electrons $\rho_i(e^-)$ in UO_2

MO		–*E*,* eV	X-ray photoelectron spectrum			Conversion spectrum			Experimental density ρ_i of the U6*p* state in e^- units	
			energy,** eV, experiment	intensity, %		energy, eV, experiment	intensity, %			
				theory	experiment		theory	experiment	$U6p_{3/2}$	$U6p_{1/2}$
OVMO	$14\gamma_8^-$	1.90	2.0(1.4)	29.3	21.4		0.1			
〃	$13\gamma_8^-$	5.87	5.3(2.5)	0.3	19.1	3.7(2.5)		7.5	0.5	0.1
〃	$12\gamma_8^+$	6.04		0.3						
〃	$10\gamma_6^+$	6.09		0.1						
〃	$7\gamma_7^+$	6.50		0.1						
〃	$11\gamma_8^+$	6.52		0.3						
〃	$10\gamma_6^-$	6.83		1.7			0.9			
〃	$11\gamma_8^-$	6.98		1.3			1.1			
〃	$12\gamma_8^-$	7.06		5.1			0.9			
〃	$6\gamma_7^-$	7.09		3.8						
〃	$9\gamma_6^-$	7.59	7.4(1.9)	0.5	7.4		0.5			
〃	$10\gamma_8^-$	7.71		4.5						
〃	$5\gamma_7^-$	7.73		2.0						
〃	$6\gamma_7^+$	8.00		0.7		8.0(4.5)	0.8	7.3		
〃	$9\gamma_6^+$	8.06		0.3						
〃	$10\gamma_8^+$	8.09		1.5			1.7			
〃	$9\gamma_8^+$	8.62	9.4(1.6)	1.9	1.7		2.5			
〃	$\sum I_i$			53.7	49.6		8.5	14.8	0.5	0.1
IVMO	$9\gamma_8^-$	18.50	17.7(3.1)	15.3	16.9	17.8(3.1)	29.2	32.3	2.7	
〃	$4\gamma_7^-$	21.01	19.6(3.0)	2.6	8.1					
〃	$8\gamma_6^-$	21.20		2.2		20.7(3.1)	2.2	3.6		0.2
〃	$5\gamma_7^+$	21.41		2.2			0.5			
〃	$8\gamma_8^+$	21.41	22.4(3.2)	4.4	6.9		0.7			
〃	$8\gamma_6^+$	21.84		2.1						
〃	$8\gamma_8^-$	22.83	23.8(3.3)	10.1	9.9	23.9(3.4)	15.8	9.3	0.8	
〃	$7\gamma_6^-$	28.63	27.9(3.5)	7.3	7.3	27.9(3.4)	43.1	37.7		1.6
〃	Sat		31.1(2.3)		1.3	31.2(2.5)		2.3		0.1
〃	$\sum I_i$			46.2	50.4		91.5	85.2	3.5	1.9
〃	$7\gamma_6^+$	45.17	47.0(6.0)	~9.7			~0.1			

Notes: $\sum I_i$ are the total line intensities and densities of the U6*p* electrons.

* For comparison with the experimental data, the calculated energies (Table 1) are shifted by 1.9 eV in the absolute value (downward) to negative values.

** The energies were obtained by resolution of the spectra into individual lines. The halfwidths, eV, of the lines are given in parentheses.

from the experimental data. The experimental and calculated binding energies of some kinds of electrons agree satisfactorily (Table 2), to a lesser extent for the middle part of the spectrum ($4\gamma_7^-$–$8\gamma_8^-$) of the IVMO electrons. Earlier [5] we analyzed the structure of the X-ray photoelectron spectrum of the IVMO electrons of UO_2 using the results of nonrelativistic calculations in the X_α approximation. This allowed qualitative identification of the fine structure of the X-ray photoelectron spectrum of uranium dioxide at energies within 0–24 eV as a result of the fact that the relativistic effects for the most part provide strong separation of the $U6p_{1/2}$ component, while the main structural features in the energy region within 0–24 eV remain unchanged. Taking into account the relativistic effects allows identification in this work of the structure of the X-ray photoelectron spectrum throughout the 0–40 eV range.

For example, the intensity of the narrow line at

1.9 eV is due mainly to the U5*f* electrons, and that of the outer valence band, to electrons of the outer valence U5*f*, 6*d*, 7*s*, 7*p* and O2*p* AOs of the neighboring atoms and, to a minor extent, to electrons of the inner valence U6*p* AO. The fact that the U5*f* electrons directly participate in chemical bonding, losing to a minor extent their *f* nature, was experimentally proved. Indeed, the experimental ratios of the intensities of the band of the OVMO electrons with (and without) account of the line of weakly bound U5*f* electrons and IVMO were estimated at 0.98 (0.56), which somewhat differs from the corresponding theoretical values of 1.16 (0.53) (Table 2). It should be noted that 15% of the value in parentheses is accounted for by the U5*f* electrons. Since the U5*f* AOs virtually are not involved in formation of the IVMO, one reason for the observed difference between these values can be an increased oxygen content in the oxide UO_{2+x}, which decreases the experimental intensity of the line of the U5*f* electrons not involved in chemical bonding. Under assumption that, e.g., the OVMO band intensity is due exclusively to the $U6d^17s^25f^3$ and $2O2p^4$ electrons, and IVMO, to the $U6p^6$ and $2O2s^2$ electrons in UO_2, the corresponding theoretical intensity ratio can be estimated at 1.15, which slightly exceeds the experimental value of 1.03 [25]. However, if we assume that the intensity of the OVMO band is due exclusively to the $U6d^27s^25f^2$ and $2O2p^4$ electrons in UO_2, and that of the IVMO bond, to the $U6p^6$ and $2O2s^2$ electrons in UO_2, the theoretical intensity ratio can be estimated at 0.87, which is slightly smaller than the experimental value [25]. Taking into account the measurement error, we can state that these results at least do not contradict the assumed direct participation of the U5*f* electrons in chemical bonding, and the results of the relativistic calculations fairly adequately reflect the partial density of states of the U5*f* electrons (Table 2). Thus, approximately one U5*f* electron directly participates in chemical bonding, and vacant U5*f* states are located near the absorption edge (Table 1). This is in qualitative agreement with the $O_{4,5}$(U) X-ray emission [12] and $O_{4,5}$(U) XANES data for UO_2 [26].

In the region of the X-ray photoelectron spectrum of the IVMO electrons, the best agreement was obtained only in the case of the $9\gamma_8^-$, $8\gamma_8^-$, and $7\gamma_6^-$ IVMOs characterizing the width of the spectrum of these electrons. Since the theoretical and experimental total relative intensities are comparable, it can be assumed that the calculated energies of the $4\gamma_7^-$–$8\gamma_6^+$ IVMOs substantially differ from the corresponding experimental energies (Table 2).

The results of nonrelativistic calculations for the UO_8^{12-} cluster with O_h symmetry and the experimental differences in the binding energies of the outer and inner electrons of uranium [27], as well as of UO_3 (see, e.g., [5, 28]), allow construction of the molecular orbital scheme in the MO LCAO approximation (Fig. 2). This scheme demonstrates the real structure of the X-ray photoelectron spectrum of UO_2. In this approximation, it is possible to formally distinguish between the antibonding $9\gamma_8^-$ (5) and $8\gamma_6^-$ (6) and the corresponding bonding $8\gamma_8^-$ (8) and $7\gamma_6^-$ (9) IVMOs, as well as, in certain approximation, quasiatomic $4\gamma_7^-$, $5\gamma_7^+$ (6), $8\gamma_8^+$, $8\gamma_6^+$ (7), and $7\gamma_6^-$ IVMOs associated mainly with the O2*s* and $U6p_{1/2}$ electrons. These experimental data suggest that the energies of the quasiatomic IVMOs associated mainly with the O2*s* AO should be close in magnitude. Indeed, the spectrum of the O1*s* electrons of UO_2 shows that their chemical nonequivalence should not exceed 0.3 eV, since the corresponding line is symmetrical, with a halfwidth Γ = 1.6 eV. The binding energy should be equal to ~22.5 eV, since E_0 = 508 eV, and the binding energy E_b of the O1*s* electrons of UO_2 was estimated at 530.5 eV (Fig. 2). These data only partially agree with the theoretical esimations. From ΔE_U = 360.6 eV and ΔE_1 = 362.9 eV follows Δ_1 = 2.3 eV [5]. Since the difference in the energies of the $7\gamma_6^-$ (9) and $9\gamma_8^-$ electrons of the IVMOs was estimated at 10.2 eV, and calculations in [29] and experiment in [27] yielded ΔE_{so}(U6*p*) = 10.0 eV for the spin–orbit coupling of the U6*p* level in the atom, the disturbance Δ_1 can be estimated at 0.2 eV. This is smaller than 2.3 eV derived from the difference in the binding energies of the inner and outer MOs. This difference is, evidently, due to formation of the IVMO, and such comparison may be not absolutely correct. The line width of the electrons of the bonding $8\gamma_8^-$ (8) and $7\gamma_6^-$ (9) IVMOs is somewhat smaller than that of the corresponding antibonding $7\gamma_6^-$ (9) and $9\gamma_8^-$ IVMOs. This can be due to a partial loss of the antibonding character by these MOs because of the admixed 3% of the O2*p* and 3% of U7*p* AOs, respectively (Tables 1, 2; Fig. 2; see also [5]).

The experimental data supporting formation of IVMO in UO_2 include its high-resolution conversion electron spectrum [11]. The structure of this spectrum was qualitatively identified on the basis of the characteristics of the X-ray photoelectron spectrum of UO_2, using the OVMO and IVMO concept [3–5]. This suggests that the spectral characteristics can also serve as a quantitative measure of the validity of the electronic structure of UO_2 that we calculated (Fig. 1).

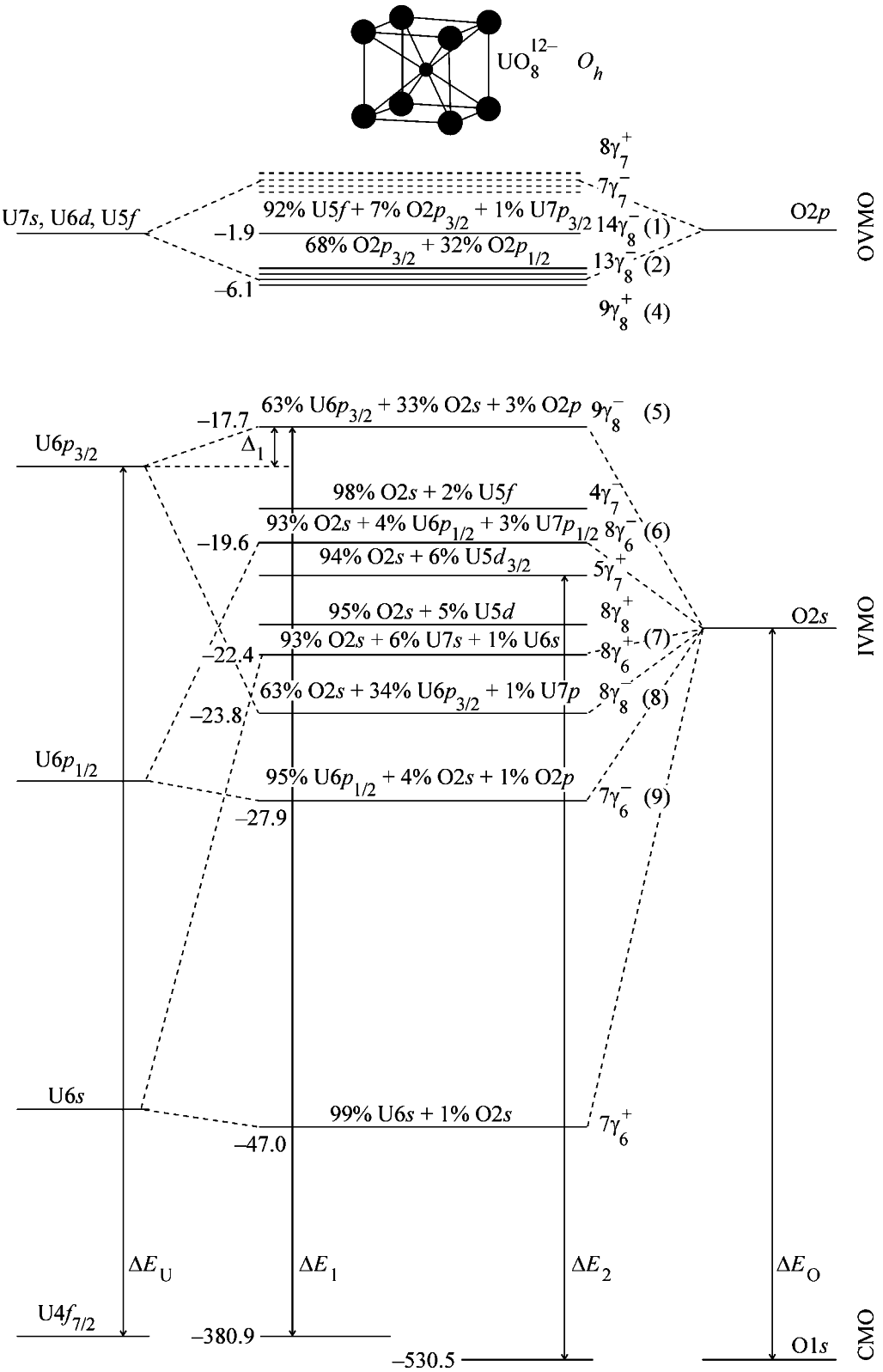

Fig. 2. MO scheme of the UO_8^{12-} (O_h) cluster, constructed using the theoretical and experimental data. The chemical shift of the levels due to formation of the cluster from individual atoms is not shown. Arrows indicate some differences in the level energies that can be measured experimentally. Figures on the left are experimental binding energies, eV, of the electrons. The energy levels are not drawn to a scale.

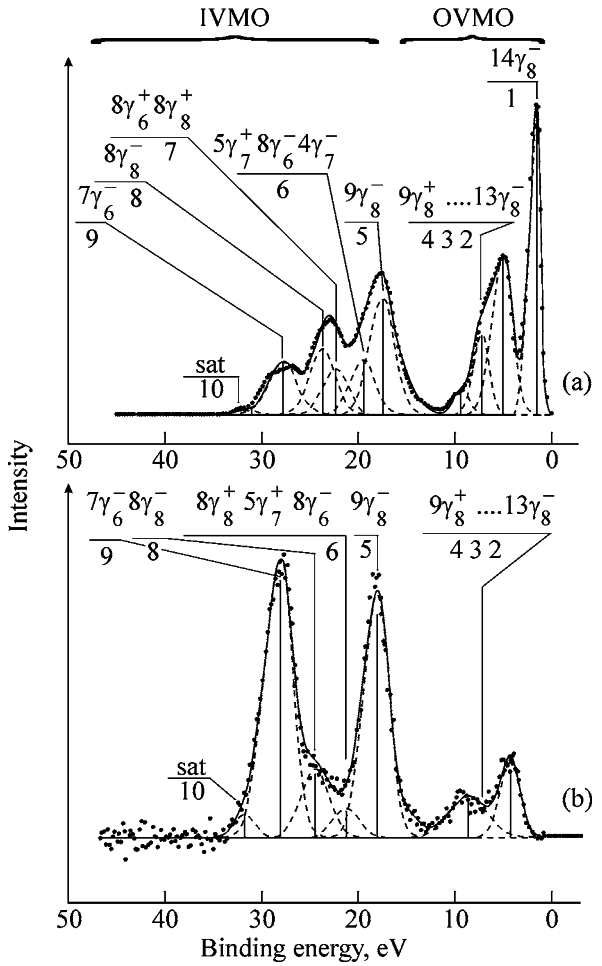

Fig. 3. (a) X-ray photoelectron and (b) conversion electron spectrum of UO_2 with the background subtracted. The vertical lines under the spectra are the corresponding expected spectra based on the theoretical and experimental data. The intensities of the spectra are in arbitrary units, and those of the theoretical spectra are normalized in %.

The fully converted transition of the $E3$ multipole of the nucleus of the ^{235m}U isomer ($T_{1/2}$ = 26.3 ± 0.2 min for UO_3) from the first excited state (spin I_1 = $1/2^+$, E_1 = 76.5 ± 0.4 eV) to the ground state of the nucleus (spin I_0 = $7/2^-$, E_0 = 0 eV) is accompanied by emission of low-energy electrons. The conversion is energetically allowed for the U6$s^2$6$p^6$5$f^3$6$d^1$7$s^2$7p^0 electrons whose shells can actively participate in formation of OVMOs and IVMOs in uranium compounds. In this case, the partial probabilities of conversion with ejection of the ($n_i l_i j_i$) electron into a continuous spectrum with the kinetic energy ε_i, α_i (EL, $I_1 \rightarrow I_0$, $n_i l_i d_i \rightarrow \varepsilon_i$), normalized to one electron (n_i is the main quantum number and l_i and j_i, orbital and total angular momentums of the electron, respectively) are proportional to the electron factor ω_e ($E3$, $n_i l_i j_i$, $h\omega$), where $h\omega$ is the excitation energy of the nucleus [23].

In this study, using the results of the electronic structure calculations for UO_2 by a relativistic method and the relative one-electron partial probabilities of conversion, we obtained the theoretical conversion electron spectrum and compared it with the corresponding experimental conversion electron spectrum (Tables 1, 2; Fig. 1). In our previous papers [13, 14] we analyzed the structure of the conversion electron spectrum of UO_3 using the partial conversion probabilities for the neutral U atom [30]. In this study, we used the corresponding parameters for the U(IV) ion [23], since in this case the theoretical and experimental data agreed better. As the conversion effect cross sections for the U6p electrons significantly exceed those for other electrons (Table 1), which are much fewer in number than the U6p electrons, the conversion electron spectrum of UO_2 reflects to a greater extent the partial density of the states of the U6p electrons in this compound. The effect cross section for the U6$p_{1/2}$ electrons is 2.1 times that for the U6$p_{3/2}$ electrons. With this fact taken into account, the experimental X-ray photoelectron and conversion spectra agree satisfactorily (Fig. 1). In spite of possible errors due to the use of the results of calculations for the ground state of the cluster, as well as the errors in determination of the probabilities of conversion and in subtraction of the background [14], the experimental and theoretical conversion electron spectra qualitatively agree. Comparison of the X-ray photoelectron and conversion electron spectra allows three important conclusions. First, the U6p shell actively participates in formation of IVMO. Second, the U6p shell significantly contributes to formation of OVMO as well. Third, as expected, the U5f electrons of the $14\gamma_8^-$ (1) OVMO and electrons from quasiatomic $4\gamma_7^-$ (6), $5\gamma_7^+$ (6), $8\gamma_8^+$ (7), and $8\gamma_6^+$ (7) IVMOs are virtually not observed in the spectrum at 19.6 and 22.4 eV, and the energies of the $9\gamma_8^-$ (5), $8\gamma_8^-$ (8), and $7\gamma_6^-$ (9) IVMOs somewhat differ from the corresponding theoretical energies and are more consistent with the experimental data derived from the X-ray photoelectron spectrum (Figs. 1, 2).

For comparative quantitative analysis of the experimental and theoretical line intensities in the spectra of interest, we carried out their resolution, taking into account the scheme (Fig. 2) constructed using the experimental binding energies and theoretically calculated intensities. Table 2 and Fig. 3 present the results of identification of the structure of the X-ray photoelectron and conversion electron spectra. It is seen that the experimental binding energies of electrons in these spectra are virtually identical. At the same time, the experimental line intensities of the IVMO electrons in

many cases substantially differ from the corresponding theoretical data. The best agreement is observed for the lines of the $9\gamma_8^-$ (5) and $7\gamma_6^-$ (9) IVMOs. Using the conversion cross sections and line intensities in the conversion electron spectrum, we estimated the partial density of the U6$p_{3/2,1/2}$ electrons for UO_2 (Table 2). Based on analysis of the experimental and theoretical data, we assumed with a good reason that the intensity of the line in the conversion spectrum at 3.7 eV is due to the U6*p* electrons (e^- is the electron charge) of uranium (Tables 1, 2; Fig. 1). We found that the OVMO comprises 0.6 U6*p* electron (Table 2), which exceeds the corresponding theoretical value of 0.2 e^- (Table 1). In this case, the U6$p_{3/2}$ electrons mostly participate in the chemical bonding. For the energy region corresponding to IVMO, agreement is observed in certain cases as well. For example, the antibonding $9\gamma_8^-$ (5) IVMO comprises 2.7 U6$p_{3/2}$ electrons, which is comparable with the corresponding calculated value, 2.52 e^- (Table 1). In the case of the bonding $8\gamma_8^-$ (9) IVMO, the agreement is less close: 0.8 e^- in the experiment (Table 2) against 1.36 e^- in the theory (Table 1).

Quantum mechanical calculations predict qualitatively the pattern of variation of the line intensities in the spectra of interest with changing level energies; therefore, the initial data for the initial clusters can be adjusted so as to bring the theoretical and experimental data into agreement. It should be noted that, as shown by us previously [5], the MO lines are the broader, the greater the contribution (bonding, antibonding) from the electrons constituting their AOs. The $9\gamma_8^-$ (5) and $8\gamma_6^-$ (6) lines corresponding to antibonding IVMOs are narrower in the conversion electron spectrum than those of the bonding $8\gamma_8^-$ (8) and $7\gamma_6^-$ (9) IVMOs (Table 2). Relative narrowing of the $9\gamma_8^-$ (5) and $8\gamma_6^-$ (6) lines of IVMOs can be due to contribution from, e.g., the O2*p* and U7*p* AOs, as previously mentioned in analysis of the X-ray photoelectron spectrum, and this results in a loss of the antibonding character. Comparison of the experimental (9.3%) and theoretical (16.2%) intensities of the $8\gamma_8^-$ (8) line of IVMO shows that the contribution from the U6$p_{3/2}$ AO into this IVMO was theoretically overestimated.

The energy region corresponding to $4\gamma_7^-$ (6)–$8\gamma_6^+$ (7) IVMOs remains the most difficult to analyze. Comparison of the X-ray photoelectron and conversion electron spectra shows that the structure in this region is due mostly to the O2*s* electrons, in accordance with the calculated data. However, the calculation overestimated the degree of overlapping of the U6*p* and O2*s* AOs in formation of the $9\gamma_8^-$ (5) and $8\gamma_8^-$ (8) IVMOs and yielded a wrong sequence of the $4\gamma_7^-$ (6) and $8\gamma_6^-$ (6) IVMOs. The correct sequence of the IVMOs is of special importance for estimating the contributions from their electrons to the covalent component of the chemical bond in UO_2. The maxima (10) observed in the spectra of interest can be due, in particular, to the shake-up process accompanying the electron emission from the sample.

To conclude, our results agree satisfactorily with the experimental data, despite a number of approximations taken in calculations of the electronic structure of the UO_8^{12-} cluster with O_h symmetry, simulating the nearest surrounding of uranium in UO_2. This allowed us for the first time to reliably identify a number of lines, at least, of the top and bottom of the IVMO band. This makes these data suitable for analysis of the structure of various X-ray (Auger, emission, absorption) spectra of UO_2.

ACKNOWLEDGMENTS

The authors are grateful to D.N. Suglobov and L.G. Mashirov for submission of the samples and useful discussion.

This work was financially supported by the Russian Foundation for Basic Research (project nos. 02-03-32693 and 04-03-32892) and by the Leading Scientific Schools State Program (project no. 1763).

REFERENCES

1. Verbist, J., Riga, J., Pireaux, J.J., and Caudano, R., *J. Electron Spectrosc. Relat. Phenom.*, 1974, vol. 5, pp. 193–205.
2. Veal, B.W., Lam, D.J., Carnall, W.T., and Hoekstra, H.R., *Phys. Rev. B.*, 1975, vol. 12, no. 12, pp. 5651–5663.
3. Teterin, Yu.A., Kulakov, V.M., Baev, A.S., *et al*., *Dokl. Akad. Nauk SSSR*, 1980, vol. 255, no. 2, pp. 434–437.
4. Teterin, Yu.A., Kulakov, V.M., Baev, A.S., *et al*., *Phys. Chem. Miner*., 1981, vol. 7, pp. 151–158.
5. Tetrin, Yu.A. and Gagarin, S.G., *Russ. Chem. Rev*., 1996, vol. 65, no. 10, pp. 825–847.
6. Walch, P.F. and Ellis, D.E., *J. Chem. Phys*., 1976, vol. 65, no. 6, pp. 2387–2392.
7. Boring, M., Wood, J.H., and Moskowitz, J.W., *J. Chem. Phys*., 1975, vol. 63, no. 2, pp. 638–642.
8. Gubanov, V.A., Rosen, A., and Ellis, D.E., *Solid State Commun*., 1977, vol. 22, no. 4, pp. 219–223.

9. Zhudov, V.I., Zelenkov, A.G., Kulakov, V.M., *et al*., Abstracts of Papers, *XXX Vsesoyuznoe soveshchanie po yadernoi spektroskopii i strukture atomnogo yadra* (XXX All-Union Conf. on Nuclear Spectroscopy and Atomic Nucleus Structure), Leningrad: Nauka, 1980, p. 614.
10. Grechukhin, D.P., Zhudov, V.I., Zelenkov, A.G., *et al*., *Pis'ma Zh. Teor. Eksp. Fiz*., 1980, vol. 31, no. 11, pp. 627–630.
11. Panov, A.D., Zhudov, V.I., and Teterin, A.Yu., *Zh. Strukt. Khim*., 1998, vol. 39, no. 6, pp. 1048–1051.
12. Teterin, Yu.A., Terechov, V.A., Teterin, A.Yu., *et al*., *J. Electron Spectrosc. Relat. Phenom*., 1998, vol. 96, pp. 229–236.
13. Teterin, Yu.A., Ryzhkov, M.V., Teterin, A.Yu., *et al*., *J. Nucl. Sci. Technol*., 2002, Suppl. 3 (November), pp. 74–77.
14. Teterin, Yu.A., Ryzhkov, M.V., Teterin, A.Yu., *et al*., *Radiokhimiya*, 2002, vol. 44, no. 3, pp. 206–214.
15. Shirley, D.A., *Phys. Rev. B*, 1972, vol. 5, no. 12, pp. 4709–4714.
16. Sidorenko, G.A., *Kristallokhimiya mineralov* (Crystal Chemistry of Minerals), Moscow: Atomizdat, 1978.
17. Rosen, A. and Ellis, D.E., *J. Chem. Phys*., 1975, vol. 62, no. 8, pp. 3039–3049.
18. Adachy, H., *Technol. Rep. Osaka Univ*., 1977, vol. 27, nos. 1364–1393, pp. 569–576.
19. Gunnarsson, O. and Lundqvist, B.I., *Phys. Rev. B*, 1976, vol. 13, no. 10, pp. 4274–4298.
20. Pyykko, P. and Toivonen, H., *Acta Acad. Aboensis B*, 1983, vol. 43, no. 2, pp. 1–50.
21. Varshalovich, D.A., Moskalev, A.N., and Khersonskii, V.K., *Kvantovaya teoriya uglovogo momenta* (Quantum Theory of Angular Momentum), Leningrad: Nauka, 1975.
22. Band, I.M., Kharitonov, Yu.I., and Trzhaskovskaya, M.B., *At. Data Nucl. Data Tables*, 1979, vol. 23, pp. 443–505.
23. Grechukhin, D.P. and Soldatov, A.A., *Yadern. Fiz*., 1978, vol. 28, no. 5(11), pp. 1206–1222.
24. Slater, J.C. and Johnson, K.H., *Phys. Rev. B*, 1972, vol. 5, no. 3, pp. 844–853.
25. Teterin, Yu.A., *Kondens. Sredy Mezhfazn. Gran*., 2000, vol. 2, no. 1, pp. 60–66.
26. Kalkowski, G., Kaindl, G., Brewer, W.D., and Krone, W., *Phys. Rev. B*, 1987, vol. 35, no. 6, pp. 2667–2677.
27. Fugle, J.S., Burr, A.F., Watson, L.M., *et al*., *J. Phys. F: Metal Phys*., 1974, vol. 4, no. 2, pp. 335–342.
28. Teterin, Yu.A. and Ivanov, K.E., *Surf. Investigat*., 1998, vol. 13, p. 623–635.
29. Huang, K.N., Aojogi, M., Chen, M.N., Graseman, B., and Mark, H., *At. Data Nucl. Data Tables*, 1976, vol. 18, pp. 243–291.
30. Grechukhin, D.P. and Soldatov, A.A., *Yadern. Fiz*., 1976, vol. 23, no. 2, pp. 273–281.